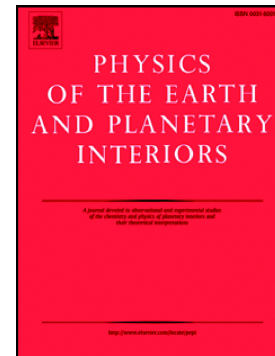


Journal Pre-proof

A full-vector paleomagnetic secular variation record from 55,000 to 33,000 cal. years BP from Río Valdéz glaciolacustrine outcrop (Tierra Del Fuego, Argentina)

Pedro Palermo, Claudia Gogorza, María J. Orgeira, María De Bernardi, María A. Irurzun, Ana M. Sinito, Romina Sancí, Andrea Coronato



PII: S0031-9201(21)00126-6

DOI: <https://doi.org/10.1016/j.pepi.2021.106768>

Reference: PEPI 106768

To appear in: *Physics of the Earth and Planetary Interiors*

Received date: 22 January 2021

Revised date: 14 May 2021

Accepted date: 30 June 2021

Please cite this article as: P. Palermo, C. Gogorza, M.J. Orgeira, et al., A full-vector paleomagnetic secular variation record from 55,000 to 33,000 cal. years BP from Río Valdéz glaciolacustrine outcrop (Tierra Del Fuego, Argentina), *Physics of the Earth and Planetary Interiors* (2018), <https://doi.org/10.1016/j.pepi.2021.106768>

This is a PDF file of an article that has undergone enhancements after acceptance, such as the addition of a cover page and metadata, and formatting for readability, but it is not yet the definitive version of record. This version will undergo additional copyediting, typesetting and review before it is published in its final form, but we are providing this version to give early visibility of the article. Please note that, during the production process, errors may be discovered which could affect the content, and all legal disclaimers that apply to the journal pertain.

© 2018 © 2021 Elsevier B.V. All rights reserved.

**A FULL-VECTOR PALEOMAGNETIC SECULAR VARIATION RECORD
FROM 55,000 TO 33,000 CAL. YEARS BP FROM RÍO VALDÉZ
GLACIOLACUSTRINE OUTCROP (TIERRA DEL FUEGO, ARGENTINA)**

Pedro Palermo¹, Claudia Gogorza¹, María J. Orgeira², María De Bernardi¹, María A. Irurzun¹,
Ana M. Sinito¹, Romina Sanci², Andrea Coronato³

¹Centro de Investigaciones en Física e Ingeniería del Centro de la Provincia de Buenos Aires (CIFICEN- CONICET - UNCPBA - CICPBA), Pinto 399, (7600) Tandil, Argentina.

²Instituto de Geociencias Básicas, Aplicadas y Ambientales de Buenos Aires (IGEBA- CONICET), Facultad de Ciencias Exactas y Naturales (Universidad de Buenos Aires), Intendente Güiraldes 2160, Pabellón II, Piso 1, Ciudad Universitaria (C1428EGA), CABA, Argentina

³Centro Austral de Investigaciones Científicas (CADIC-CONICET). B. Houssay 200, 9410 Ushuaia, Argentina.

*Corresponding author at e-mail address: claudiagogorza65@gmail.com

Abstract

High-resolution paleomagnetic investigations were performed on Río Valdez outcrop at the Fagnano Lake, central Isla Grande de Tierra del Fuego, southernmost South America. Our aims were to develop a full-vector paleomagnetic secular variation (PSV) record and establish paleomagnetic chronostratigraphy for the outcrop based on radiocarbon dating and the correlation of the PSV record with other dated PSV records in the region. We detected two distinct anomalous directional intervals at 35,400 and 33,800 cal. years BP and at 41,500 and 39,000 cal. years BP, which could be associated with Mono Lake and Laschamp excursions.

Rock magnetic investigations revealed slight changes in concentration, mineralogy, and magnetic grain size along the sedimentary sequence, but the reconstruction of past direction and relative paleointensity variations in the geomagnetic field remained feasible. The record provides new insights into the behavior of the geomagnetic field at high latitudes in the Southern Hemisphere, about which very little is currently known.

Keywords: paleomagnetic secular variation, excursion, Late-Pleistocene, sediments, Patagonia

1. Introduction

The main geomagnetic field and its secular variation can tell us a great deal about the Earth's deep interior, and main-field and secular-variation models (particularly spherical harmonic models) are widely used in studies on the dynamics of the outer layers of the Earth's core. The data on which such models are based must be of the highest quality and distributed as homogeneously as possible worldwide (Barraclough, 1991). According to Lisé-Pronovost (2013), global stacks are truly derived from a majority of records located in the Northern Hemisphere (e.g., GLOPIS-75, Laj et al., 2004; SINT-200, Guyodo and Valet, 1996) and geomagnetic field models lack calibration data from the Southern Hemisphere to better understand the core geodynamics (e.g., Korte et al., 2005; Roberts, 2008; Korte and Constable, 2011; Pavón-Carrasco et al., 2014). Besides, high-resolution records of the paleomagnetic field made available a series of appropriate markers for global-scale correlation of paleomagnetic and paleoclimatic archives. In particular, the interval 30,000–50,000 cal. years BP comprising significant evidence of the variability of the climate during the Marine Isotope Stage (MIS) 3 justifies more detailed studies (Blanchet et al., 2006). Over the last two decades, we have contributed to building a more comprehensive record of Pleistocene-Holocene geomagnetic variability in southwestern Argentina and filling the gaps in data distribution for the Southern Hemisphere (Gogorza et al., 2012; Lisé-Pronovost et al.,

2013; Gogorza et al., 2018; Palermo et al., 2019; to cite some of the latest papers) by studying lake sediments, evaluating rock magnetic parameters, and yielding increasingly precise chronostratigraphy for these records. This study presents paleomagnetic data from a Late-Pleistocene glaciolacustrine record located at the Fagnano Lake ($54^{\circ} 35' S$; $67^{\circ} 20' W$), central Isla Grande de Tierra del Fuego, southernmost South America. In particular, we searched for distinct features in the secular variation of the geomagnetic field and, possibly field excursions, which can be useful as chronostratigraphic markers. This paleosecular variation record would provide a correlation tool for this region and geomagnetic time-series data for a previously unrepresented part of the globe.

2. Study area

The Fagnano Lake is located in central Isla Grande de Tierra del Fuego, southernmost South America. It extends W-E along latitude $54^{\circ} 33' S$, between longitudes $67^{\circ} 13'$ and $68^{\circ} 48' W$ along 100 km, and has a maximum depth between 260–290 m below the mean lake level. Most of its surface is placed in the Argentine territory but some of it is in Chile, where its emissary, the Azopardo river, drains towards the Almirantazgo Fjord, Magellan Straits. The present lake extends in half-graben, pull-apart basins developed along the Sudamerica-Scotia transforming boundary plates (Menichetti et al., 2008), repeatedly occupied by ice during the Pleistocene (Coronato et al., 2009). The studied site is located close to the Río Valdez mouth, on the southeast coast of Fagnano Lake, where an exposed continuous profile of *circa* 9 m thick lacustrine sediments ($54^{\circ} 35' S$; $67^{\circ} 20' W$) crops out (Fig. 1) (Sanci et al., 2020). Based on ground magnetic and resistivity surveys, a maximum E-W extension of ~ 220 m and a minimum thickness of ~ 20 m were determined for the complete sedimentary sequence (Prezzi et al., 2019). This thickness suggests that the Fagnano Lake glacier was probably active during MIS 4. This interpretation is also supported by fossil peat ages obtained from the

surrounding glaciodeltaic deposits by Bujalesky et al. (1997) and till deposits by Coronato et al. (2009).

The defined lithofacies in the studied profile (Sanci et al., 2020) made it possible to delineate the evolution of the paleolacustrine environment during the deposition of the studied record (Fig. 2). The base of the outcrop is represented by Unit A, composed of silty-clayey sediments distributed in two lithofacies formed by deposition from suspension, one of them during periods with no current activity in the water body and the other one under alternating deposition conditions of low energy tractive currents. Unit B comprises a succession of fine sand silty-clay layers with thin and very thin bedding; two lithofacies were recognized, and they were generated when incomplete small sand ripples were formed in a mud-silt substratum and when wavy stratification was formed due to slightly alternating conditions. Unit C, at the top of the lake sequence, is composed of clay and silt sediments. The observed lithofacies represent successively massive sediments deposited from suspended load and slight bed load movements that form different sedimentary structures such as ripple beds or lenticular bedding. All the sediments and their characteristics are compatible with a glacial lacustrine record. Also, the succession of sedimentary facies represents an exceptionally continuous outcropping record of lake sediments. The total absence of fossils indicates lake water temperature related to direct contact with ice mass (Sanci et al, 2020); consequently, any kind of bioturbation can be expected. The characteristics of the diamictic sediments that cover the outcrop indicate that they were laid down by ice, thus forming a till. These diamictic sediments were not sampled for paleomagnetic studies.

3. Methods

3.1 Field work

Two parallel profiles, a few meters apart from each other, were sampled at the Río Valdez outcrop during the 2012 Austral summer: Río Valdez 1 (RV1) and Río Valdez 2 (RV2), about 6.5 m and 4.5 m thick, respectively. Standard paleomagnetic sampling boxes (external size 2.2x2.2x2.2 cm and internal volume of 8 cm³) were pushed into the sediments at about 2 cm intervals at the site (n=224 for RV1 and n=144 for RV2) and then transported in boxes to the laboratory (see Subsection 3.2 below) for magnetic measurements.

3.2 Paleomagnetic and rock magnetic measurements

Paleomagnetic and rock magnetic measurements were performed at the laboratory of Paleomagnetism and Paleoenvironmental Magnetism in Tandil (CIFICEN, Buenos Aires, Argentina). Magnetic susceptibility was measured at low (κ_{low}) and high frequency (κ_{high}) with the MS2 Bartington susceptibility instrument equipped with the MS2B dual-frequency sensor at 0.47 kHz and 4.7 kHz. The frequency dependence of low-field susceptibility was estimated by the frequency-dependent factor (κ_{fd}), in terms of the low frequency and high-frequency measurements (Dearing, et al., 1999). The natural remanent magnetization (NRM, D, and I) was measured using a MR6A Dual Speed Spinner Magnetometer. The orientation of the samples was preserved with respect to the reference line pre-marked in the field. The NRMs of all samples were demagnetized and measured sequentially in alternating magnetic fields (AF) of 10, 15, 20, 25, 30, and 40 mT, which reduced most initial NRMs to less than 20% of their initial values. The selected samples were also demagnetized and measured at 60, 80 mT, and 100 mT. The results of stepwise AF demagnetization were plotted and analyzed using Zijderveld diagrams (Zijderveld, 1967). The characteristic remanent magnetization (ChRM), i.e., paleomagnetic inclination, declination, intensity, and maximum angular deviation (MAD), were calculated by principal component analysis using the least square method (Kirschvink, 1980). After each demagnetization cycle, anhysteretic remanent

magnetization (ARM) was applied to a 0.05 mT bias field, with an in-line single-axis direct current (DC) coil, combined with an axial peak AF of 100 mT. Finally, Isothermal Remanent Magnetization (IRM) for all samples was acquired at room temperature in increasing steps up to 1.2 T reaching saturation (SIRM), and in increasing steps back until the magnetic remanence was canceled using an IM-10-30 Pulse Magnetizer (ASC Scientific).

Subsequently, AF demagnetizations of ARM and SIRM were measured using the same steps as for NRM demagnetization. Different magnetic properties and inter-parametric ratios were used to characterize the sediments in terms of type, concentration, and grain size of magnetic minerals. Magnetic susceptibility was used as a first-order indicator of the concentration of magnetic (sensu lato) minerals. S_{ratio} was determined by dividing the back field measurement IRM_{-300mT} with SIRM (Thompson and Oldfield, 1986). Combined magnetic parameters were calculated (SIRM/ κ and ARM/SIRM). In addition, the median destructive field of the NRM (MDF_{NRM}) was determined as a first estimate of relative magnetic grain-size variations.

Susceptibility vs. temperature measurements (k-T curve) under air were carried out using a Bartington susceptibility meter equipped with a furnace. The pilot samples were heated up to about 700 °C at a heating rate of 20 °C/min and then cooled at the same rate. Hysteresis loops were measured in fields up to a maximum of 1 T using a Molspin VSM (Vibration Sample Magnetometer) at the Institute of Basic, Applied, and Environmental Geosciences of Buenos Aires (IGEBA; Buenos Aires, Argentina) to determine the domain state of the magnetic minerals (Day et al., 1977; Dunlop, 2002).

3.3 Age-depth model

The age model used for this study was based on the radiocarbon age-depth model constructed by Sanci et al. (2020) and refined by tuning the PSV records of Río Valdez outcrop to the PSV records of Potrok Aike (Lisé-Pronovost et al., 2013), a high-resolution paleomagnetic

record constructed from the long sedimentary archive of Laguna Potrok Aike (PASADO-ICDP) covering the last 51.2 kyr. cal. BP.

4. Results

4.1 Rock magnetic results

Rock magnetic parameters were investigated to characterize the magnetic properties of the sediments and evaluate the stability of paleomagnetic records. The concentration magnetic parameters (κ , NRM, ARM, and SIRM) vs depth, along with the sedimentary units, are plotted in Fig. 3.a. The sediments are generally weakly magnetized with κ , NRM, ARM, and SIRM intensities in the range of $9 - 23 \times 10^{-5}$ SI ($8 - 23 \times 10^{-5}$ SI), 0.2 – 14 mA/m (0.2 – 60 mA/m), except for three samples with NRM of 206, 237, and 514 mA/m, 3 – 10 mA/m (0.1 – 30 mA/m), and 101 – 243 mA/m (57 – 1400 mA/m) for RV1 (RV2), respectively. An up-core decrease (increase) and high-frequency variations in κ , NRM, and ARM (SIRM) are observed in Unit A. In particular, κ , NRM, and ARM display conspicuous oscillations superimposed on the general trend. In Unit B, all concentration magnetic parameters show oscillations although these changes are less noticeable than in Unit A, except for NRM in RV1. Finally, in Unit C, all parameters show small variations and follow an increasing trend at the top of the unit. Further above, significantly decreased values for all concentration-dependent magnetic parameters are observed in RV2 associated with unstratified deposits at the top of the outcrop. Interestingly, in general, all magnetic parameters show more pronounced fluctuations in RV2. A detailed analysis of the magnetic parameters obtained allows us to determine the variety of magnetic minerals in the studied material. The following analysis is presented for the whole sequence in general, focusing on some levels with distinctive characteristics that differ from the means. The κ_{fd} (not shown), a parameter sensitive to magnetic grains in superparamagnetic (SP) grain size range (Maher, 1988; Dearing, 1999), is highly fluctuating

and varies between 0.003 and 0.05, suggesting no presence of SP grains. S_{ratio} are typically higher than 0.9, indicating that the mineral magnetic composition is dominated by a soft coercivity component (e.g. (titano)magnetite). Anyway, lower values of S_{ratio} are observed in Units A and B, which suggests a slightly higher presence of a high coercivity mineral in addition to the (titano)magnetite (Fig. 3.a and b).

As detailed by Nilsson et al. (2018), ARM/SIRM is a parameter sensitive to the remanent carrying stable single domain (SSD)/PSD grains (Maher, 1988) and varies inversely with magnetic grain size (Maher and Taylor, 2007); higher values indicate finer magnetic grain size (SSD, PSD) and lower values correspond to coarse grains (MD). ARM/SIRM ranges from 0.01 to 0.05 (0.005 to 0.03) in RV1 (RV2) (Fig. 3.a and b). ARM/SIRM shows a decreasing trend, suggesting a decrease in the abundance of SSD/PSD-sized magnetic grains.

Besides, the SIRM/ κ ratio is a parameter sensitive to magnetic grains in the PSD range. Such inferences cannot be drawn when other ferrimagnetic minerals such as greigite are present. Indeed, Roberts (1995) showed that greigite is characterized by large SIRM/ κ values.

SIRM/ κ varies from 1 to 5 kA/m, except for two samples that reach ca. 20 kA/m at the top part of RV2. SIRM/ κ shows a much more even pattern, which points to a more evenly distributed abundance of the PSD-sized magnetic grains (Fig. 3.b). In particular, the presence of ferrimagnetic iron sulfides (greigite) at Unit C of RV2 (300-302 cm, Fig. 3.b) is supported by high values of SIRM/ κ , an increase in the remanence coercivity (up to 40 mT), and a slight drop in the S_{ratio} .

The SIRM of the pilot samples was reached below ca. 300 mT, indicating a magnetic assemblage dominated by low coercivity minerals (Fig. 4.a). Progressive removal of SIRM by back-field demagnetization indicates that coercivities (B_{CR}) vary approximately between 31 and 42 mT (27 and 40 mT) in RV1 (RV2), suggesting that a low coercive magnetic mineral, such as magnetite of pseudo-single domain size (PSD), might be predominant within the

sediments (e.g., Dunlop and Özdemir, 1997). Higher values are observed between 772 and 803 cm in RV1 and towards the upper part (<10 cm) of RV2, in both cases reaching ca. 55 mT (Fig. 3.a and b). These values, not characteristic for pure magnetite, could be caused by the presence of partially oxidized (titano)magnetite (Roberts and Turner, 1993) and/or antiferromagnetic minerals in low concentrations, or by the decrease in the size of the grain. The increase of ARM/IRM in these parts of the profiles supports the latter hypothesis. The Day plot of hysteresis loop parameters (Fig. 5) for the pilot samples exhibits M_{RS}/M_S ratios ranging between 0.1 and 0.4 and H_{CR}/H_C ratios varying between 3.1 and 3.9, lying roughly on a (titano)magnetite grain size mixing line within the PSD field (Dunlop, 2002). There appears to be a slight displacement toward higher values of H_{CR}/H_C in a group of samples. These results show that, as is usually the case in sediment mixtures, the average grain size corresponds to the PSD range. It should be noted, however, that such observation could also derive from a mixture of two populations of single domain and multidomain grains (Blanchet et al., 2006). The continuous thermomagnetic experiments showed that the pilot samples present two magnetic phases. In the shown sample, the first magnetic mineral fraction has a Curie temperature of around $567 \pm 19^\circ\text{C}$ and $452 \pm 47^\circ\text{C}$, compatible with (titano)magnetite with variable titanium content (Prévoit et al., 1983). The second magnetic phase has a Curie temperature of about 675°C , suggesting the presence of a hard magnetic carrier like hematite in low proportion (Dunlop and Özdemir, 1997) (Fig. 4.b).

4.2 Paleomagnetic directions

The AF demagnetization results of representative samples are illustrated and analyzed using Zijderveld diagrams (Zijderveld, 1967), also known as vector end plot diagrams. ChRM information is extracted from the orthogonal projection of the Zijderveld diagram using least square analysis (Kirschvink, 1980). The Zijderveld plot for selected samples of RV1 and RV2

(Fig. 6) shows that the viscous remanence magnetization –if present at all– is eliminated by applying demagnetization fields of 5 mT. Most of the samples have a single paleomagnetic direction that is demagnetized between 10–40 mT, which demagnetizes toward the origin. The ChRM MAD values are generally $<5^\circ$, indicating a well-defined component magnetization. Beyond 941 cm (RV1) and for the top 10 cm (RV2), we could not retrieve reliable PSV records due to the scattered behavior of NRM intensity. Inclination and declination data below 968 cm are too noisy and many samples did not exhibit stable demagnetization paths; MAD also shows large scatter and an increase to $10\text{--}20^\circ$. Therefore, the ChRM data below 941 cm are not interpreted in the present study. Besides, samples in both profiles that show scatter behavior during the AF demagnetization were also discarded. The MDF is defined as the value of the peak AF required to reduce the remanence intensity to half its initial value and mostly depends on the composition and/or grain size of the minerals carrying these remanences. MDF_{NRM} lies between 21 and 35 mT and 13 and 38 mT in RV1 (mean = 21 mT) and RV2 (mean = 19 mT), respectively (Fig. 3.b) and indicates a fairly stable remanent magnetization. Stacking of individual curves is commonly employed on multiple paleomagnetic records to obtain more reliable estimates of the temporal variation in the directions of the geomagnetic field (Gogorza et al., 2012 and references therein). The mean inclination is -57.5° for RV1 and -60.9° for RV2; inclinations range between -32.8° and -71.8° and between -38.2° and -79.8° , respectively. Declination varies between -109° and 35.6° in RV1 and -66° and 62.7° in RV2 (Fig. 7). The average inclination (-58.6°) is lower than the inclination (-70.4°) of the field produced by an axial dipole at the site latitude and results from a series of intervals with lower inclinations (I-1 to I-5, Fig. 7). The inclination lows I-1, I-2, and I-3 depart around 30° from the GAD (vertical dashed line in Fig. 7) whereas I-4 and I-5 depart up to approximately 20° and 18° , respectively. I-1 is the interval displaying the lowest inclination values, and it is found from 35,500 to 33,700 cal. years BP with a

minimum inclination recorded at 34,600 cal. years BP (-38.6°). The other interval with inclinations deviating around 30° from the GAD is I-2, and it represents the interval from 37,700 to 35,700 cal. years BP. Besides, I-4 is the longest feature ranging from 41,600 to 38,500 cal. years BP, showing two narrow peaks and a small drop in between. Finally, the other two less prominent features, I-4 and I-5, are recorded at 43,950 (-50.2°) and 45,700 (-52.6°) cal. years BP, respectively. Rapid fluctuations in declination observed between 46,500 and 45,000 cal. years BP (D-5) and 41,000 and 39,000 cal. years BP (D-3) are probably associated with low inclinations, I-5 and I-3, respectively. Minor upward swings are observed in declination in the intervals 44,300–43,500 and 35,700–33,700 cal. years BP (D-4 and D-1), which could be associated with the anomalous inclinations I-4 and I-1, respectively. We found no anomaly in declination in the vicinity of 37,700–35,700 cal. years BP inclination anomaly (I-2).

4.3 Relative Paleointensity

The use of normalized NRM intensity to evaluate relative paleointensity (RPI) variations is conventionally based on the reliability criteria established by Banerjee et al. (1981) and King et al. (1982, 1983) and further refined by Tauxe (1993). The concentration of magnetic minerals in the sediments between 55,000 and 33,000 cal. years BP can be considered relatively stable, suggesting that the trends in the RPI within this period could reflect the relative intensity variations in the paleomagnetic field. In order to meet the criteria for uniformity in terms of concentration (Tauxe, 1993), those samples whose concentrations are beyond a factor of 10 were rejected. Paleointensity variability was estimated by normalizing the NRM to κ , ARM and SIRM. The NRMs after 10 mT AF demagnetization were normalized by dividing the NRM by either ARM or SIRM demagnetized at the same AF level and then renormalized by dividing the values by their mean value. $\text{NRM}_{10\text{mT}}/\kappa$,

$\text{NRM}_{10\text{mT}}/\text{ARM}_{10\text{mT}}$, $\text{NRM}_{10\text{mT}}/\text{SIRM}_{10\text{mT}}$ are displayed in Fig. 8. Due to the markedly decreasing trend in the relative abundance of small magnetic grains observed in both profiles (Fig. 3.b), the use of the ARM as a normalizer may not be suitable. On the contrary, both κ and IRM are not affected in the same way as the ARM (Fig. 3.a) and are therefore likely more appropriate for these sediments. It is observed in Fig. 8 that $\text{NRM}_{10\text{mT}}/\kappa$, and $\text{NRM}_{10\text{mT}}/\text{SIRM}_{10\text{mT}}$ show similar results both in terms of fluctuation and amplitude, whereas $\text{NRM}_{10\text{mT}}/\text{ARM}_{10\text{mT}}$ displays a more pronounced long-term trend and lower amplitude fluctuations, in particular from 40,500 to 55,000 cal. years BP.

We carried out spectral analyses and a coherence test of normalized remanences and normalization parameters to confirm that the normalized records are free from environmental influence. Spectral analysis was performed using the MCCLEAN algorithm (Heslop and Dekkers, 2002). Coherence tests were carried out according to the methods described by Tauxe and Wu (1990) by means of MATLAB 6.1 software. The best normalization parameter is the one that displays no coherence with its normalizer parameter (Tauxe, 1993; Tauxe and Wu, 1990). At the 95% confidence level, the $\text{NRM}_{10\text{mT}}/\text{SIRM}_{10\text{mT}}$ normalized intensity is not coherent with its normalizer except at periods corresponding to the interval 450-850 years. However, neither $\text{NRM}_{10\text{mT}}/\text{SIRM}_{10\text{mT}}$ nor $\text{SIRM}_{10\text{mT}}$ shows significant power in these periods. Therefore, they do not represent the influence of climate on lithology (Fig. 9). In agreement with the sediment cores from Laguna Potrok Aike (Gogorza et al., 2012), we consider that $\text{SIRM}_{10\text{mT}}$ should be the best normalizer for the sediments. We also show a closer resemblance between NRM and SIRM demagnetization curves compared to ARM demagnetization curves (Supplementary Material). This behavior was observed in most of the analyzed pilot samples taken along the whole core. We conclude that $\text{SIRM}_{10\text{mT}}$ is the most appropriate normalizer to construct the RPI proxies in these sediments.

RPI mostly fluctuates between 0.4 and 1.2 for the period 55,000–41,900 cal. years BP (Fig.

8). We note a significant drop in paleointensity in the vicinity of the observed inclination anomaly I-4 at 41,500–40,400 cal. and a slight fall in the interval 46,200–45,200 years BP, which would coincide with the anomalous inclination I-5. From 40,400 cal. years BP to the present, we observe a clear increase and conspicuous oscillations. In particular, a remarkable minimum is displayed around 35,500–34,500 cal. years BP. However, we do not observe any anomaly in paleointensity in the vicinity of I-2 inclination anomaly.

5. Discussion

5.1. Some highlights about magnetic parameters

The mixed magnetic mineralogy determined in all sedimentary units is described in Subsection 4.1. However, given the variation in the magnetic parameters obtained throughout the studied sedimentary sequence, some environmental considerations can be suggested. It is interesting to note that, in general, all magnetic parameters show more pronounced fluctuations in RV2. Also, the top of Unit C in this profile, which represents the youngest record of the sequence, shows both a decrease in S_{ratio} and an increase in B_{CR} (Fig. 3.a and 3.b). These magnetic signals indicate a relatively more oxidizing environment, which could be explained by the position of this profile in the sedimentary basin, close to the lake coast, and/or a decrease in lake water level.

Magnetic parameters in Unit A show high-frequency variations in κ , NRM, and ARM (SIRM), displaying conspicuous oscillations superimposed on the general trend. Also, a trend to higher κ and B_{CR} (and lower S_{ratio}) would indicate mixed magnetic particles slightly different from the rest of the sequence (Fig. 3.a). These magnetic variations are associated with lithofacies formed under alternating deposition from suspension during periods with no current activity in the water body and deposition with low-energy tractive currents. Very fine gravel intercalated between the thin facies could correspond to dropstones from ice-drifted

processes (Sanci et al., 2020). Based on the age model, the top of Unit A would be assigned to *circa* 55,000 cal. years BP. Therefore, the geological and magnetic evidence indicates that this unit could have developed under a different climatic scenario from that of the rest of the sequence, possibly related to the end of Marine Isotope Stage (MIS) 4 or more likely the beginning of MIS 3 (Lisiecki and Raymo, 2005). Unit B also shows a variation in magnetic parameters (Fig. 3.a and 3.b), although these changes are less conspicuous than those of the other units. A certain cyclicity can be perceived, which is associated with the rhythmites detected in the stratigraphic description. Another interesting level is represented in Unit C, namely a level with greigite detected in RV2 profile (Fig. 3.d). This finding is supported mainly by high SIRM/ κ values associated with an increase in the remanence coercivity (up to 40 mT); this level with a diagenetic mineral is representative of particular environmental conditions (Fig. 3.b). Considering an authigenic origin, greigite is an intermediate iron sulfide on the polysulfide pathway to pyrite (Roberts et al. 2011, among others). Greigite has become a common component in both lacustrine anoxic sedimentary environments (Blanchet et al. 2009, among others). It is formed below the oxic-to-anoxic transition zone (OATZ). Below the OATZ, degradation of organic matter must involve a reaction with sulfates. To form greigite in a lacustrine system, the lake water must be stratified and the sediment/water interface must be under reducing conditions (Evans and Heller, 2003). In the studied deposit, lake stratification may have been caused by an increase in the lake level and/or low wind speeds, which prevent water mixture and/or unusual low winter temperatures. Taking into account its depth into the sequence and the age model, this level could represent prevailing 35,000 cal. years BP conditions. The aforementioned rise in the water lake level is not clearly related to any conspicuous global climate change but could be the consequence of a local process or represent some of the climatic variations occurring during MIS 3 (Lisiecki and Raymo, 2005).

5.2 Mono Lake and Laschamp Excursions

Apart from reversals of the geomagnetic field, wide departures from its usual value have been observed in the geomagnetic field direction at a single locality. Such departures, when the field does not appear to change polarity but returns to its previous state, have been named geomagnetic excursions. Geomagnetic excursions during Brunhes chron, such as Mono Lake (Teanby et al., 2002; Nowaczyk et al., 2013; Lund et al., 2017); Laschamp (Teanby et al., 2002; Thouveny et al., 2004; Nowaczyk et al., 2013; Lund et al., 2017; Usapkar et al., 2018); Denmark (Abrahamsen and Knudsen, 1979); Norwegian-Greenland (Nowaczyk et al., 2013; Usapkar et al., 2018); Blake (Zhu et al., 1994; Thouveny et al., 2004), and Icelandic Basin excursions (Thouveny et al., 2004), have been identified worldwide. The youngest recorded excursions are of particular interest because they offer the potential for identifying them in several places on the Earth's surface and investigating their global morphology (Merrill and Mc Elhinny, 1983; Korte et al., 2019). In sedimentary sequences, it is possible to obtain a good continuous record of a transition if the sedimentation has been rapid. In marine sediments, the magnetic record is locked in over a 10 to 30 cm range so that the magnetic signal recorded by them is fixed. However, sediment records have proved to be one of the most valuable sources of information on the transitional behavior of the geomagnetic field (Merrill and Mc Elhinny, 1983).

The PSV recorded in the sediments of Río Valdez outcrop contains three main intervals of anomalous directions: 35,400–33,800 cal. years BP, 41,500–39,000 cal. years BP, and 46,600–45,300 cal. years BP (Fig. 7). We consider that the youngest of these anomalous PSV intervals (I-1) could be associated with the Mono Lake excursion, the large directional swing (I-3) at intermediate ages could be related to Laschamp geomagnetic excursion, and the oldest but less conspicuous one (I-5) could correspond to the directional swing recorded at 46,000

cal. years BP at Laguna Potrok Aike (Lisé-Pronovost et al., 2013). According to Lisé-Pronovost et al. (2013), the last one could represent an important geomagnetic feature in the Southern Hemisphere. The center ages of these intervals of anomalous directions are 34,600, 40,250, and 45,650 cal. years BP, which implies a good agreement with the recent dating of Mono Lake excursion ($34,100 \pm 300$ cal. years BP, Lund et al., 2017) and Laschamp geomagnetic excursion ($41,100 \pm 350$ cal. years BP, Lascu et al., 2016; Lund et al., 2017). Further support for the interpretation of I-1 being the Mono Lake excursion is the presence of a coeval declination swing (D-1) and a relative paleointensity minimum (Fig. 8), as expected during a geomagnetic excursion. Similar departures are observed in inclination values. The inclination swing I-2 can be associated with Laschamp geomagnetic excursion. In this case, a large declination swing (D-2) and a minimum in RPI validate our interpretation. Finally, a coeval declination swing (D-5) is associated with I-5, although the behavior in paleointensities is quite ambiguous.

5.3 A comparison of global-scale paleomagnetic directions

To compare the global-scale paleomagnetic directions, the following available directional records are displayed: Potrok Aike ($51^{\circ}58'S$ $70^{\circ}22'W$) (Lisé-Pronovost et al., 2013); MD94-103 ($45^{\circ}35'S$ $86^{\circ}31'E$) (Mazaud et al., 2002); Crevice Cave ($37^{\circ}40'N$ $89^{\circ}50'W$) (Lascu et al., 2016); Wega (Macri et al. 2005), and Hawaiian lava flows ($19^{\circ}29'N$ $154^{\circ}54'W$) (Teanby et al., 2002). In particular, a very good centennial-scale agreement is observed with the inclination record of Laguna Potrok Aike, as expected due to its location at a distance of ~ 400 km. However, declination does not show a very similar pattern. Differences in the amplitude of variations could, in turn, be related to the different sedimentation rates and lock in depths of the different records. The inclination records are generally consistent and most peak values of Río Valdez can be correlated among the records (I-1 to I-5). In the case of declination,

following the numbers of inclination, the main patterns are identified as D-1, D-3, D-4, and D-5. The inclination low event I-5 in Río Valdez (Fig. 10.a) is associated with the sharp declination swing D-5 (Fig. 10.b). Similar direction swings are observed in Potrok Aike (Lisé-Pronovost et al., 2013), Crevice Cave (Lascu et al., 2016), MD94-103 (Mazaud et al., 2002), and Hawaiian lava flows (Teanby et al., 2002). The comparison reveals a good correlation between the inclination lows I-1, I-2, I-3, I-4, I-5 (Fig. 10.a), (with, however, different amplitudes for I-2 and I-5) and the declination swings D-2 and D-5 (Fig. 10.b). Concerning the directional feature (I-5 and D-5) at 46,000 cal. years BP, which according to Lisé-Pronovost et al. (2013) seems to be mainly observed in the Southern Hemisphere, a similar pattern is displayed in Crevice Cave, located about 38°N.

5.3 A comparison of global-scale paleomagnetic intensities

In Fig. 10.c, the relative paleointensity record from Río Valdéz is compared for the period 55,000–33,000 cal. years BP with the lacustrine records of Laguna Potrok Aike (Lisé-Pronovost et al., 2013), the marine records from the Indian and Atlantic sectors of the Southern Ocean (MD94-103; Mazaud et al., 2002, and SAPIS; Stoner et al., 2002), from the western Equatorial Pacific (MD97-2134; Blanchet et al., 2006), and the WEGA stack near Antarctica (Macrì et al., 2005). This comparison also includes a speleothem geomagnetic record from North America (Crevice Cave; Lascu et al., 2016) and the VADMs derived from Black Sea sediments (Nowaczyk et al., 2013) and lacustrine sediments of Lake Baikal (Peck et al., 1996). Three periods can be clearly identified. A decreasing trend from 55,000 to ~45,500 cal. years BP is followed by a small increase from 45,500 to 41,000 cal. years BP. From 41,000 to 33,000 cal. years BP, the intensity shows an oscillating behavior superimposed on a value that doubled the intensity of the previous intervals. Although the records are generally consistent, it should be noted that the described decreasing trend, from

55,000 to ~45,500 cal. years BP, is not as noticeable in the records from Argentina as observed in the remaining records. In particular, an intensity low (P-3) in Río Valdéz (Fig. 10.c) is associated with the inclination low event I-3 (Fig. 10.b) and the sharp declination swing D-3 (Fig. 10.b). Similar direction swing and intensity low are observed in the records: MD94-103 (Mazaud et al., 2002), MD97-2134 (Blanchet et al., 2006), and Crevice Cave (Lascu et al., 2016). Besides, the low P-1 in Río Valdéz (Fig. 10.c) associated with the low inclination event I-1 (Fig. 10.b) and the less conspicuous declination swing D-1 (Fig. 10.b) is displayed in Potrok Aike (Lisé-Pronovost et al., 2013) and MD94-103 (Mazaud et al., 2002). The intensity lows P-1 and P-3 are also observed in the RPI of SAPIS (Stoner et al., 2002) and ODP 1089 (Stoner et al., 2003). Some temporal shifts are observed and could be linked to the uncertainties of the respective chronologies. Additionally, the minimum in intensity at about 46,000 cal. years BP, which is related to the inclination low event I-5 (Fig. 10.b) and the declination swing D-5, is absent at Río Valdéz (Fig. 10.c). However, it is displayed at Potrok Aike (Lisé-Pronovost et al., 2013), SAPIS (Stoner et al., 2002), and ODP 1089 (Stoner et al., 2003). Based on the comparative analysis, we cannot discard a rock-magnetic influence on the RPI recorded in the sediments from Río Valdéz for the period 55,000 to 47,000 cal. years B, although all the stringent requirements for RPI studies were fulfilled.

6. Conclusions

We performed a rock magnetic and paleomagnetic study of Late-Pleistocene sediments of Río Valdez outcrop in Southern South America. On the basis of our analysis, we constructed a full-vector PSV record for the interval 55,000 to 33,000 calibrated years BP. A global-scale paleomagnetic intensity and direction comparison of the Río Valdéz record supports the validity of the geomagnetic signal. We confirm the existence of two intervals of anomalous paleomagnetic directions, at $34,600 \pm 800$ cal. years BP and at $40,250 \pm 1250$ cal. years BP,

which could be associated with evidence of Mono Lake and Laschamp Excursion in the records of Río Valdéz. It is important to point out that this is the first record with these characteristics at this latitude.

The following are the supplementary data related to this article.

Supplementary Table 1. Modelled age for RV1 and RV2 profiles of Río Valdéz outcrop, including ^{14}C date and calibrated ages (RV1-22; RV1-17; RV2-5; RV2-11; RV2-15). Modified from Sanc. et al. (2020).

Supplementary material 1

Acknowledgments

This research was funded by the projects PIP N° 112-201201-00573 - Comisión Nacional de Investigaciones Científicas y Técnicas de la República Argentina (CONICET – Argentina; Director: Claudia Gogorza) and PICT 2012-068 - Agencia Nacional de Promoción Científica (ANPCyT – MINCyT, Argentina; Director: Andrea Coronato). Laboratory tasks were supported by Universidad Nacional del Centro de la Provincia de Buenos Aires. Diego Quiroga and Ramiro López provided assistance with fieldwork and sampling.

AUTHORSHIP STATEMENT

P. Palermo: Conception and design of study, acquisition of data, analysis and/or interpretation of data, drafting the manuscript, revising the manuscript critically for important intellectual content, approval of the version of the manuscript to be published.

C.S.G. Gogorza: Conception and design of study, acquisition of data, analysis and/or interpretation of data, drafting the manuscript, revising the manuscript critically for important intellectual content, approval of the version of the manuscript to be published.

María J. Orgeira: Conception and design of study, acquisition of data, analysis and/or interpretation of data, revising the manuscript critically for important intellectual content, approval of the version of the manuscript to be published.

María De Bernardi: Analysis and/or interpretation of data, approval of the version of the manuscript to be published.

M.A. Irurzun: Analysis and/or interpretation of data, approval of the version of the manuscript to be published.

Ana M. Sinito: Analysis and/or interpretation of data, approval of the version of the manuscript to be published.

Romina Sanci: Support for the stratigraphic characterization of Río Valdez outcrop, approval of the version of the manuscript to be published.

Andrea Coronato: Sedimentary exposure discovered and conception of its paleoenvironmental significance, acquisition of data, revising the manuscript critically for important intellectual content, approval of the version of the manuscript to be published.

conflicts of interests

The authors report no conflicts of interests

References

- Abrahamsen, N., Knudsen, K. L., 1979. Indication of a geomagnetic low-inclination excursion in supposed middle Weichselian interstadial marine clay at Rubjerg, Denmark. *Physics of the Earth and Planetary Interiors*, 18, 238–246.
- Banerjee, P. K., Butterfield, R., 1981. *Boundary Element Methods in Engineering Science*, McGraw-Hill Book Company (UK), 452 pp.
- Barracough, D. R., 1991. Modelling the geomagnetic main field and recent secular variation. *Geophysical & Astrophysical Fluid Dynamics*, 60, 3–35.
- Blanchet, C. L., Thouveny, N., de Garidel-Thoron, T., 2006. Evidence for multiple paleomagnetic intensity lows between 30 and 50 ka. BP from a western Equatorial Pacific sedimentary sequence. *Quaternary Science Reviews*, 25, 1039–1052.

- Blanchet, C. L., Thouveny, N., Vidal, L., 2009. Formation and preservation of greigite (Fe_3S_4) in sediments from the Santa Barbara Basin: implications for paleoenvironmental changes during the past 35 ka. *Paleoceanography*, 24, PA2224, doi:0.1029/2008PA001719.
- Bujalesky, G., Heusser, C., Coronato, A., Roig, C., Rabassa, J. 1997. Pleistocene glaciolacustrine sedimentation at Lago Fagnano, Andes of Tierra del Fuego, Southernmost South America. *Quaternary Science Reviews*, 16 (1-2), 767–778.
- Coronato, A., Seppälä, M., Ponce, J. F., Rabassa, J. 2009, Glacial geomorphology of the Pleistocene Lake Fagnano ice lobe, Tierra del Fuego, southern South America. *Geomorphology*, 112, 67–81.
- Day, R., Fuller, M., Schmidt, V. A., 1977. Hysteresis properties of titanomagnetites: grain size and composition dependence. *Physics of the Earth and Planetary Interiors*, 13, 260–267.
- Dearing, J. A., 1999. *Environmental Magnetic Susceptibility: Using the Bartington MS2 System*. Chi Pub., Kenilworth. 54 pp.
- Dunlop, D. J., 2002. Theory and application of the Day plot (M_r/M versus H_c/H_c): 2. Application to data for rocks, sediments and soils. *Journal of Geophysical Research*, 107 (B3), 2057.
- Dunlop, D. J., Özdemir, Ö. 1997. *Rock Magnetism: Fundamentals and Frontiers*. Cambridge University Press, Cambridge, New York.
- Evans, M., Heller, F., 2003. *Environmental Magnetism. Principles and Applications of Enviromagnetics*, 317 pp. Academic Press, Elsevier.
- Gogorza, C. S. G., Irurzun, M. A., Sinito, A. M., Lisé-Pronovost, A., St-Onge, G., Haberzettl, T., Ohlendorf, C., Kastner, S., Zolitschka, B., 2012. High-resolution paleomagnetic records from Laguna Potrok Aike (Patagonia, Argentina) for the last 16,000 years. *Geochemistry, Geophysics, Geosystems*, 13, 12.

- Gogorza, C. S. G., Irurzun, M. A., Orgeira, M. J., Palermo, P., Llera, M., 2018. A continuous Late Holocene paleosecular variation record from Carmen Lake (Tierra del Fuego, Argentina). *Physics of the Earth and Planetary Interiors*, 280, 40–52.
- Guyodo, Y., Valet, J. P., 1996. Relative variations in geomagnetic intensity from sedimentary records: the past 200 thousand years. *Earth and Planetary Science Letters*, 143 (1–4), 23–36.
- Heslop, D., Dekkers, M., 2002. Spectral analysis of unevenly spaced time series using CLEAN: Signal recovery and derivation of significance levels using a Monte Carlo simulation, *Physics of the Earth and Planetary Interiors*, 130, 103–116, doi:10.1016/S0031-9201(01)00310-7.
- King, J., Banerjee, S. K., Marvin, J., Ozdemir, O., 1982. A comparison of different magnetic methods for determining the relative grain size of magnetite in natural materials: Some results from lake sediments, *Earth and Planetary Science Letters*, 59, 404–419.
- King, J. W., Banerjee, S. K., Marvin, J., 1983. A new rock magnetic approach to selecting sediments for geomagnetic paleointensity studies: Application to paleointensity for the last 4000 years. *Journal Geophysical Research*, 88, 5911–5921.
- Kirschvink, J. L., 1980. The least-squares line and plane and the analysis of paleomagnetic data. *Geophysical Journal International*, 62, 699–718.
- Korte, M., Constable, C., 2011. Improving geomagnetic field reconstructions for 0–3 ka. *Physics of the Earth and Planetary Interiors*, 188 (3–4), 247–259.
- Korte, M., Genevey, A., Constable, C. G., Frank, U., Schnepp, E., 2005. Continuous geomagnetic field models for the past 7 millennia: 1. A new global data compilation. *Geochemistry, Geophysics, Geosystems*, 6, Q02H15.
- Korte, K., Brown, M. C., Panovska, S., Wardinski, I., 2019. Geomagnetic Excursions: Results from Global Field Models. *Frontiers in Earth Science*, 7, 86, doi: 10.3389/feart.2019.00086.

- Laj, C., Kissel, C., Beer, J., 2004. High resolution global paleointensity stack since 75 kyrs (GLOPIS-75) calibrated to absolute values. In: Channell, J. E. T., Kent, D. V., Lowrie, W., Meert, J. G. (Eds.), *Timescales of the Paleomagnetic Field*. AGU Geophysical Monograph, 145.
- Lascu, I., Feinberg, J., Dorale, J. A., Cheng, H., Lawrence Edwards, R., 2016. Age of the Laschamp excursion determined by U-Th dating of a speleothem geomagnetic record from North America. *Geology*, 44(2), G37490.1.
- Lisé-Pronovost, A., St-Onge, G., Gogorza, C., Haberzettl, T., Precca, M., Kliem, P., Francus, P., Zolitschka, B., 2013. High-resolution paleomagnetic secular variations and relative paleointensity since the Late Pleistocene in southern South America. *Quaternary Science Reviews*, 71, 91–108.
- Lisiecki, L. E., Raymo, M. E. 2005. A Pliocene–Pleistocene stack of 57 globally distributed benthic $\delta^{18}\text{O}$ records. *Paleoceanography*, 20(1), doi:10.1029/2004PA001071.
- Lund, S., Benson, L., Negrini, R., Liddicoat, J., Mensing, S., 2017. A full-vector paleomagnetic secular variation record (PSV) from Pyramid Lake (Nevada) from 47–17 ka: Evidence for the successive Mono Lake and Laschamp Excursions. *Earth and Planetary Science Letters*, 458, 120–122.
- Macri, P., Sagnotti, L., Dinares-Turell, J., Caburlotto, A., 2005. A composite record of Late Pleistocene relative geomagnetic paleointensity from the Wilkes Land Basin (Antarctica). *Physics of the Earth and Planetary Interiors*, 151, 223–242.
- Maher, B. A., 1988. Magnetic properties of some synthetic submicron magnetites. *Geophysical Journal International*, 94 (1), 83–96.
- Maher, B. A., Taylor, R. H., 2007. Formation of ultrafine-grained magnetite in soils. *Nature*, 336, 368–370.

- Mazaud, A., Sicre, M., Ezat, U., Pichon, J., Duprat, J., Laj, C., Kissel, C., Beaufort, L., Michel, E. Turon, J. L., 2002. Geomagnetic-assisted stratigraphy and sea surface temperature changes in core MD94-103 (Southern Indian Ocean): possible implications for north– south climatic relationships around H4. *Earth and Planetary Science Letters*, 201, 159–170. doi: 10.1016/S0012-821X(02)00662-3
- Menichetti, M., Lodolo, E., Tassone, A., 2008. Structural geology of the Fuegian Andes and Magallanes fold-and-thrust belt – Tierra del Fuego Island. *Geologica Acta* 6 (1), 19–42.
- Merrill, R.T., Mc Elhinny, M.W., 1983. The earth's magnetic field. Its history, origin and planetary perspective. In: Donn, W.L. (Ed.), *International Geophysics Series*. Academic Press Inc.
- Nilsson, A., Suttie, N., Hill, M. J., 2018. Short-term magnetic field variations from the post-depositional remanence of lake sediments. *Frontiers in Earth Science*, 6. <https://doi.org/10.3389/feart.2018.00039>.
- Nowaczyk, N. R., Frank, U., Kind, J., Arz, H. W., 2013. A high-resolution paleointensity stack of the past 14 to 68 ka from Black Sea sediments. *Earth and Planetary Science Letters*, 384, 1–16.
- Palermo, P., Irurzun, M. A., Cogorza, C. S. G., Sinito, A. M., Ohlendorf, C., Zolitschka, B., 2019. Rock magnetic and paleomagnetic studies on Late-Holocene sediments from Laguna Cháltel (Patagonia, Argentina). *Journal of South American Earth Sciences*, 90, 204–215.
- Pavón-Carrasco, F. J., Osete, M. L., Torta, J. M., De Santis, A., 2014. A geomagnetic field model for the Holocene based on archaeomagnetic and lava flow data. *Earth and Planetary Science Letters*, 388, 98–109.
- Peck, J. A., King, J. W., Colman, S. M., Kravchinsky, V. A., 1996. An 84-kyr paleomagnetic record from the sediments of Lake Baikal, Siberia. *Journal of Geophysical Research*, No. B5, 11,365–11,385.

- Prérot, M., Mankinen, E. A., Grommé, S., Lecaille, A., 1983. High paleointensities of the geomagnetic field from thermomagnetic studies on rift valley pillow basalts from the Mid-Atlantic Ridge. *Journal of Geophysical Research: Solid Earth*, 88(B3), 2316–2326.
- Prezzi, C., Orgeira, M. J., Coronato, A., Quiroga, D., Ponce, J. F., Nuñez Demarco, P., Palermo, P., 2019. Geophysical methods applied to quaternary studies in glacial environments: Rio Valdez outcrop, Tierra del Fuego, Argentina. *Quaternary International*, 525, 114–125.
- Roberts, A. P., 2008. Geomagnetic excursions: knowns and unknowns. *Geophysical Research Letters*, 35, L17307.
- Roberts, A., Turner, G., 1993. Diagenetic formation of ferromagnetic iron sulphide minerals in rapidly deposited marine sediments, New Zealand. *Earth planet. Sci. Lett.*, 115, 257–273.
- Roberts, A. P., 1995. Magnetic properties of sedimentary greigite (Fe_3S_4), *Earth and Planetary Science Letters*, 134, 227–236.
- Roberts, A. P., Chang, L., Rowan, C. J., Horng, C. S., Florindo, F., 2011. Magnetic properties of sedimentary greigite (Fe_3S_4): an update, *Review of Geophysics*, 49, RG1002, doi:10.1029/2010RG000336.
- Sanci, R., Orgeira, M. J., Coronato, A., Tófaló, R., Panarello, H. O., Quiroga, D., López, R., Palermo, P., Gogorza, C., 2020. Late Pleistocene glaciolacustrine record assignable to MIS 3 at Lago Fagnano, Central Tierra del Fuego, Southern Argentina. *Quaternary Research*, doi:10.1017/qua.2020.93.
- Stoner, J., Laj, C., Channell, J. E. T., Kissel, C., 2002. South Atlantic (SAPIS) and North Atlantic (NAPIS) geomagnetic paleointensity stacks (0-80 ka): implications for inter-hemispheric correlation. *Quaternary Science Reviews*, 21, 1141–1151.

Stoner, J. S., Channell, J. E. T., Hodell, D. A., Charles, C. D., 2003. A ~580 kyr paleomagnetic record from the sub-Antarctic South Atlantic (Ocean Drilling Program Site 1089). *Journal of Geophysical Research*, 108, B5, 2244, doi:10.1029/2001JB001390.

Tauxe, L., 1993. Sedimentary records of relative paleointensities of the geomagnetic field: theory and practice. *Review of Geophysics*, 31, 319–354.

Tauxe, L., Wu, G., 1990. Normalised remanence in sediments of the western equatorial Pacific: Relatively intensity of the geomagnetic field? *Journal of Geophysical Research*, 95, 12,337–12,350.

Teanby, N., Laj, C., Gubbins, D., Pringle, M., 2002. A detailed paleointensity and inclination record from drill core SOH1 on Hawaii. *Physics of the Earth and Planetary Interiors*, 131, 101–140.

Thompson, R., Oldfield, F., 1986. *Environmental Magnetism*. Allen & Unwin Ltd, 225pp.

Thouveny, N., Carcaillet, J., Moreno, E., Leuc, G., Nérini, D., 2004. Geomagnetic moment variation and paleomagnetic excursions since ka BP: a stacked record from sedimentary sequences of the Portuguese margin. *Earth and Planetary Science Letters*, 219.

Usapkar, A., Dewangan, P., Marumdar, A., Krishna, K. S., Ramprasad, T., Badesab, F. K., Patil, M., Gaikwad, V. V., 2019. Paleomagnetic record for the past 80 ka from the Mahanadi basin, Bay of Bengal. *Journal of Asian Earth Sciences*, 151, 226–239.

Zhu, R. X., Zhou, L. P., Laj, C., Mazaud, A., Ding, D. L., 1994. The Blake geomagnetic polarity episode recorded in Chinese loess. *Geophysical Research Letters*, 21, 697–700.

Zijderveld, J. D. A., 1967. AC demagnetization of rock: analysis of results. In: Collinson, D. W., Creer, K. M., Runcorn, S. K. (Eds.), *Methods in Paleomagnetism*. Elsevier, Amsterdam, The Netherlands, pp. 254–286.

Figure 1. Location maps: (a) geographical location of Río Valdez outcrop, (b) locations of the sampling sites.

Figure 2. Stratigraphic integrated scheme from the sedimentary record of RV1 and RV2.

Figure 3. (a) Down-core variations in concentration-magnetic parameters: magnetic susceptibility (κ), NRM, ARM, SIRM, and MDF_{NRM} from RV1 and RV2 along with the sedimentary units. (b) Down-core variations in rock-magnetic parameters: SIRM/ κ , ARM/SIRM, BCR, and S_{ratio} of RV1 and RV2, along with κ and the sedimentary units.

Figure 4. Rock magnetic properties of the Río Valdez sediments: (a) Isothermal Remanent Magnetization (IRM) acquisition curves, for representative samples from RV1 and RV2. (b) Thermomagnetic curves (κ vs. T) of a pilot sample.

Figure 5. Day plot (Day et al., 1977) for the sediment samples of Río Valdez outcrop. The mixing reference lines for single and multi-domain (SD and MD) are from Dunlop (2002).

Figure 6. Normalized intensity decay curves and orthogonal vector plots for four pilot samples from RV1 and RV2, produced by stepwise AF demagnetization at 5-10 mT steps, up to a maximum field of 100 mT. Closed (open) circles denote the projection on the horizontal (vertical) plane.

Figure 7. (a) Inclination and (b) declination plots for RV1 (open squares), RV2 (closed squares), and stacked profile (orange line). (c) Latitudes of the related virtual geomagnetic pole (VGP).

Figure 8. Normalized estimates of relative paleointensity (RPI): NRM_{10mT}/κ , $NRM_{10mT}/SIRM_{10mT}$ and NRM_{10mT}/ARM_{10mT} versus Age.

Figure 9. Spectral analysis of three normalization parameters (ARM_{10mT} , $SIRM_{10mT}$ and κ) and three normalized remanences (NRM_{10mT}/ARM_{10mT} , $NRM_{10mT}/SIRM_{10mT}$ and NRM_{10mT}/κ). Coherence tests of relative paleointensity curves with respect to the normalization parameters, showing that the normalized intensity curves are generally not coherent with the normalization parameters.

Figure 10. (a) Comparison of global-scale of paleomagnetic (a) inclination, (b) declination and (c) relative paleointensity records. Directional profiles include Río Valdez (this study); Potrok Aike (Lisé-Pronovost et al., 2013); Crevice Cave (Lascu et al., 2016); Wega (Macri et al. 2005); MD94-103 (Mazaud et al., 2002), Hawaiian lava flows (Teanby et al., 2002); MD97-2134 (Blanchet et al., 2006), and Lake Baikal (52°N 106°E) (Peck et al., 1996). (c) Comparison of normalized intensity comprises the relative paleointensity from Río Valdez (this study), the marine records from the

Indian and Atlantic sectors of the Southern Ocean (MD94-103; Mazaud et al., 2002, and SAPIS; Stoner et al., 2002), from the western Equatorial Pacific (MD97-2134; Blanchet et al., 2006), the WEGA stack near Antarctica (Macrì et al., 2005), a speleothem geomagnetic record from North America (Crevice Cave; Lascu et al., 2016), the VADM_s derived from Black Sea sediments (Nowaczyk et al., 2013), and lacustrine sediments from Lake Baikal (Peck et al., 1996). Notable features of the paleomagnetic inclination (I-1 to I-5), declination (D-1 to D-5), and intensity (P-1 to P-2) are indicated. The Laschamp and Mono Lake geomagnetic excursions are underlined in green and the event at ca 46,000cal. years BP in purple (see text for details).

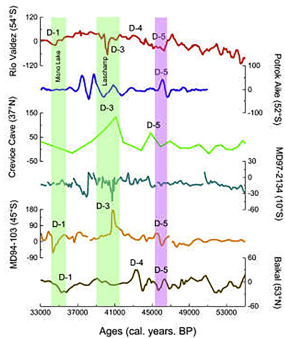
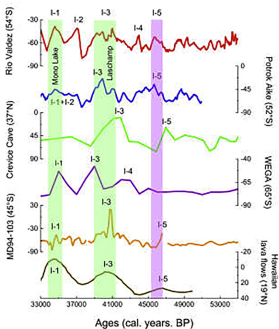
Graphical Abstract

Highlights

- We report new paleomagnetic results for the Lago Lagnano Lake, central Isla Grande de Tierra del Fuego, southernmost South America.
- The results confirm the existence of two intervals of anomalous paleomagnetic directions, which could be associated with evidence of Mono Lake and Laschamp Excursions.
- This is the first record with these characteristics reported at this latitude.



Río Valdéz Outcrop
(Argentina)



Graphics Abstract

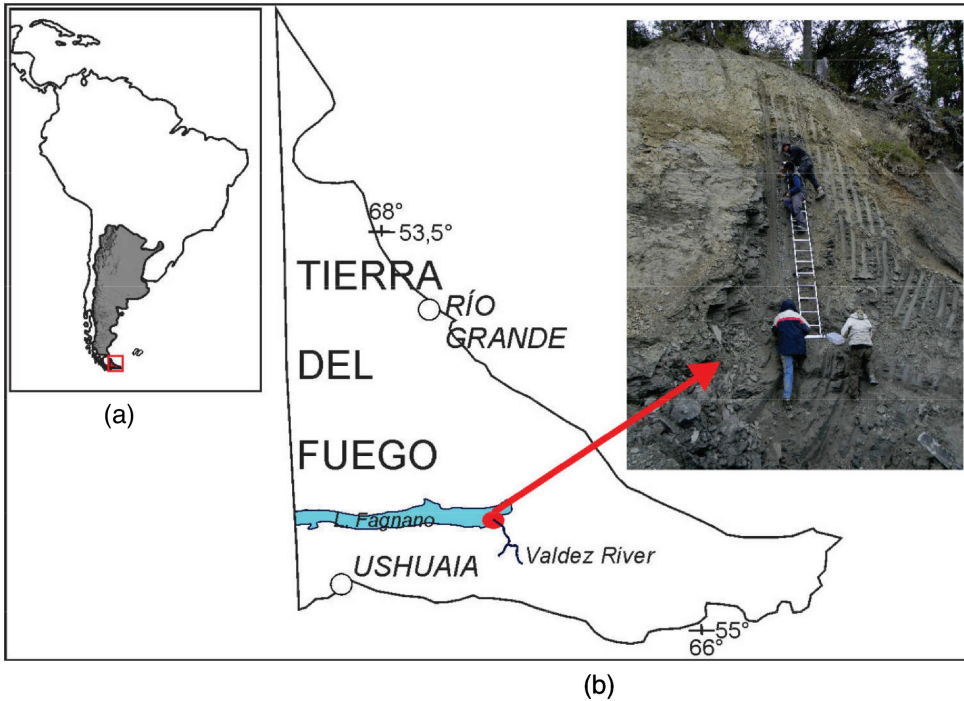
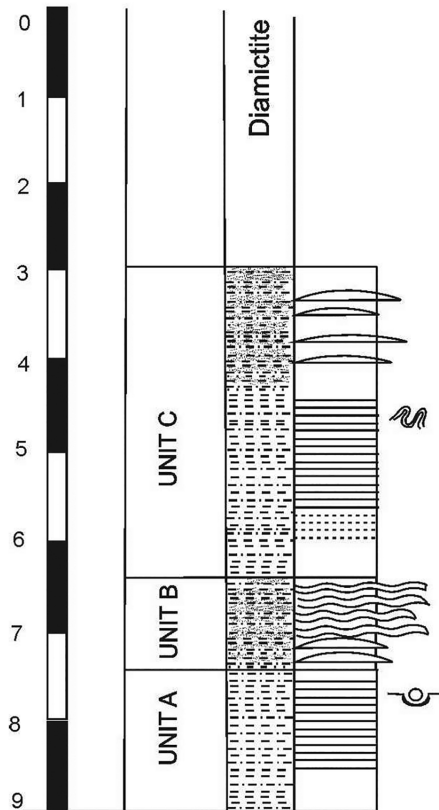


Figure 1



References

Lithology



Sand



Silt



Clay

Sedimentary Structures



Massive



Convolute



Wavy
bedding



Lamination



Dropstone



Lenticular
bedding

Figure 2

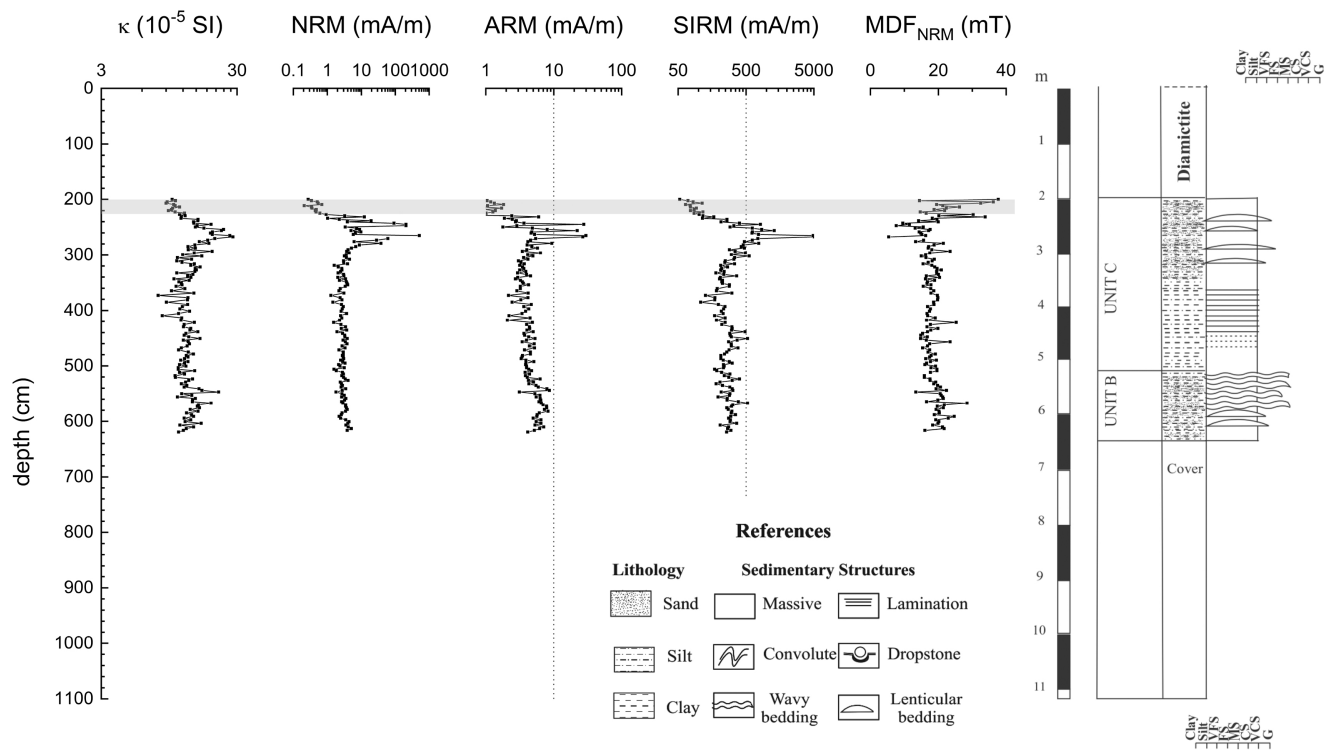
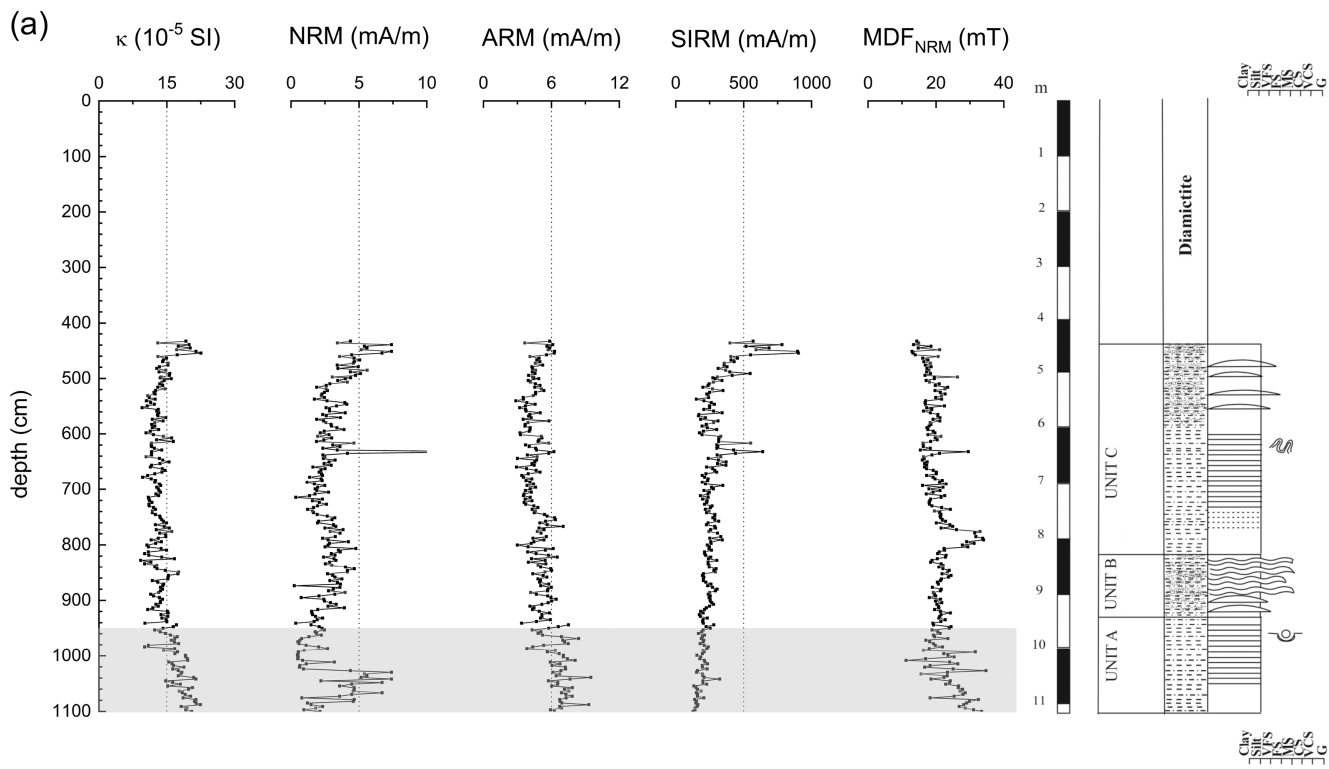


Figure 3A

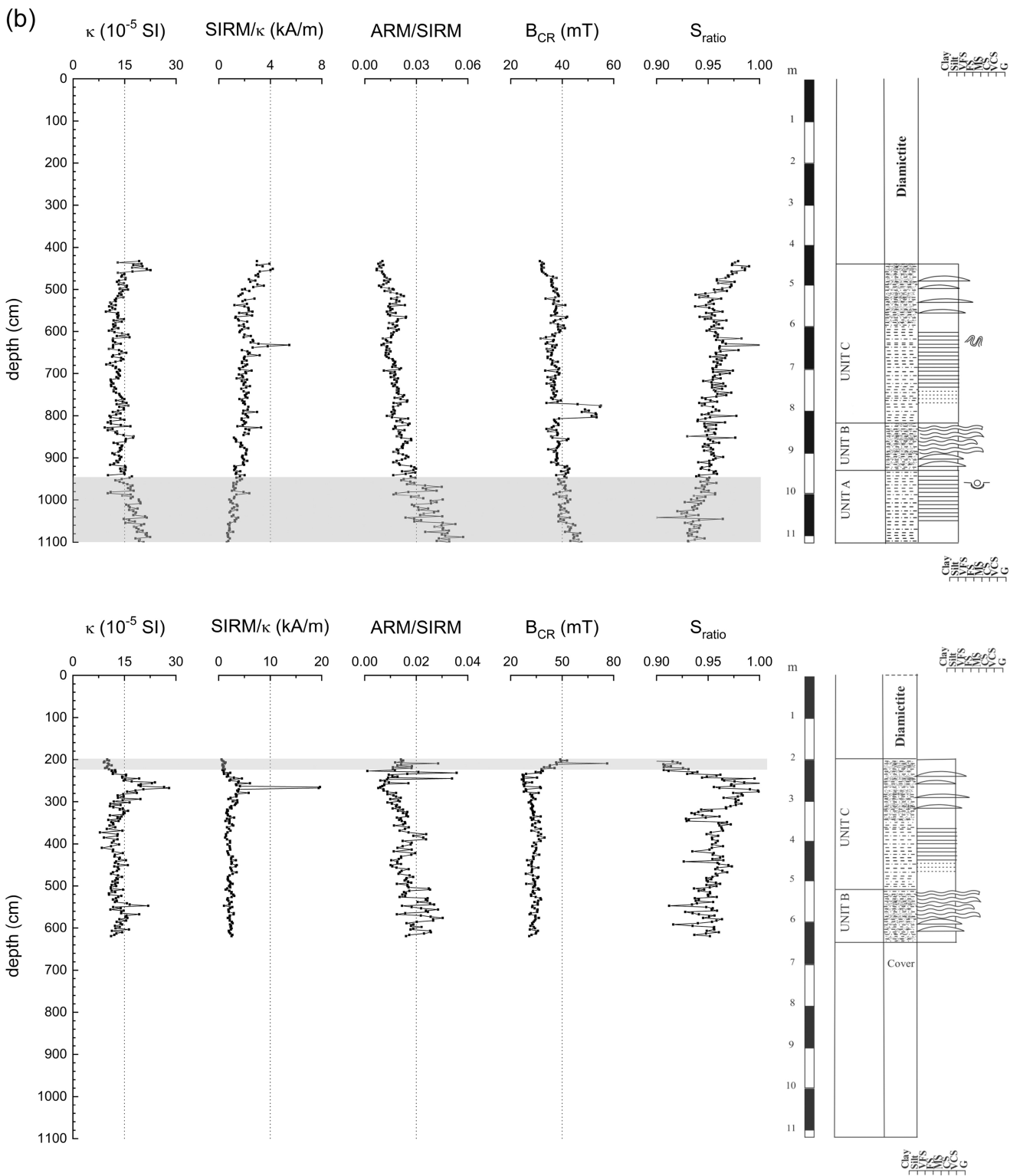


Figure 3B

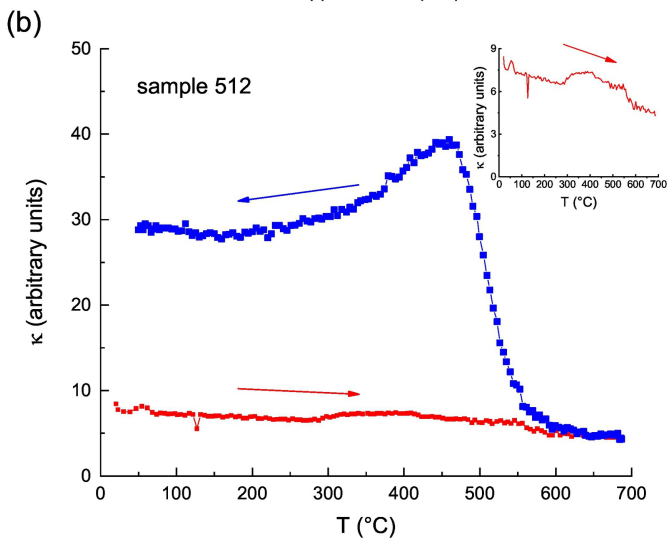
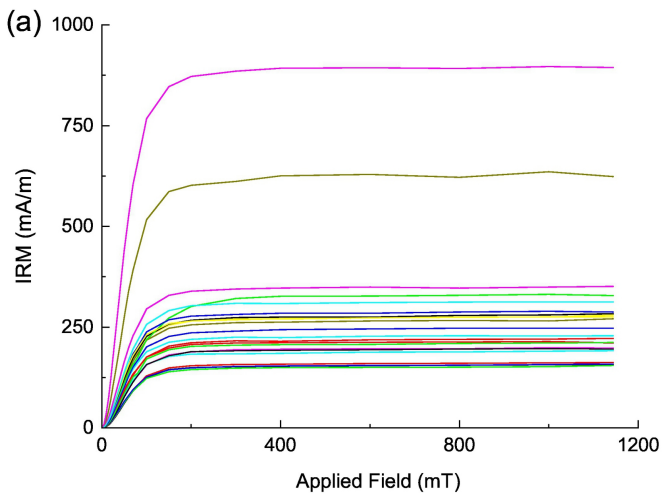


Figure 4

Theoretical Day plot curves for magnetite

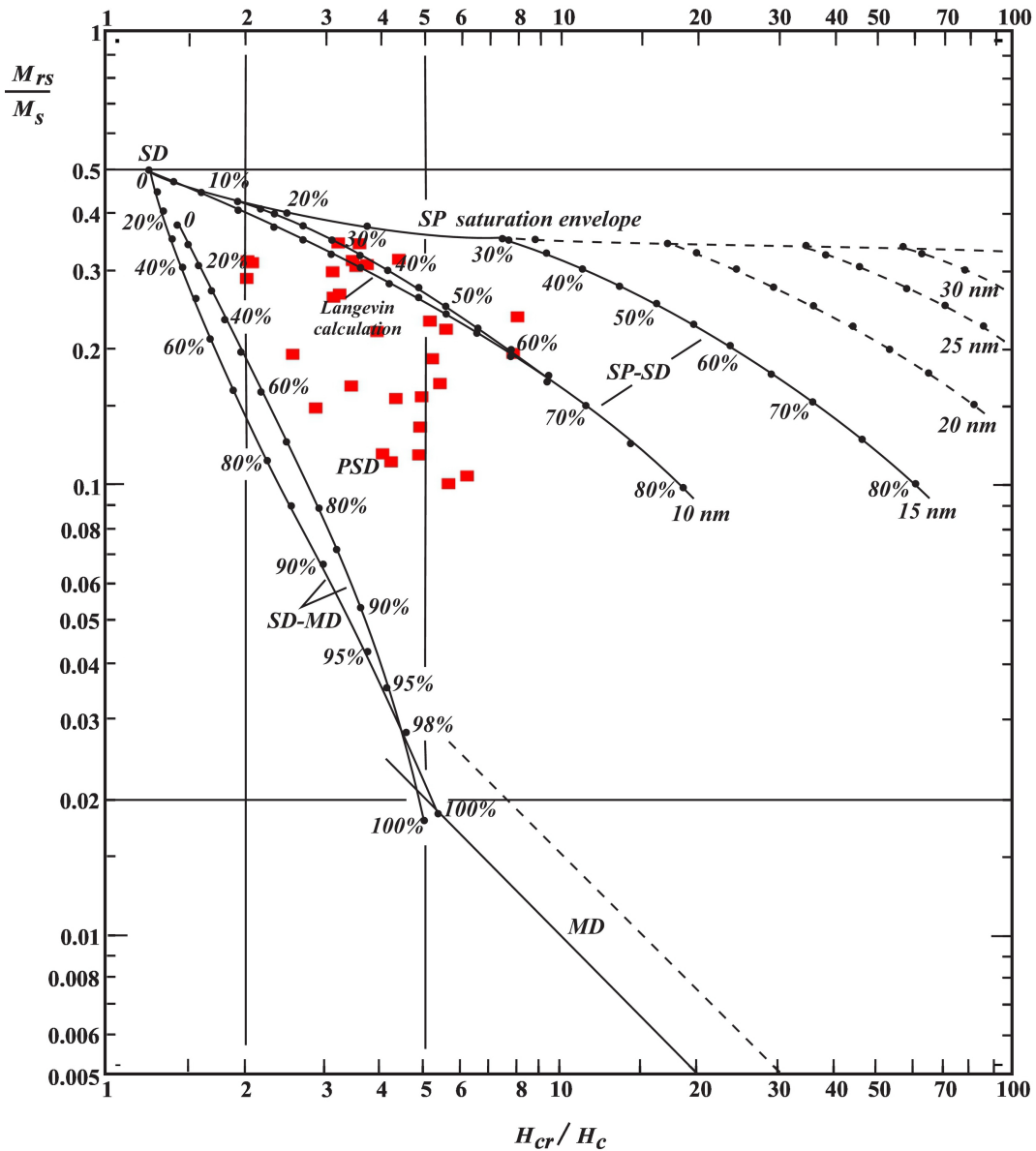
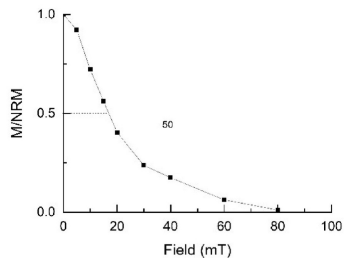
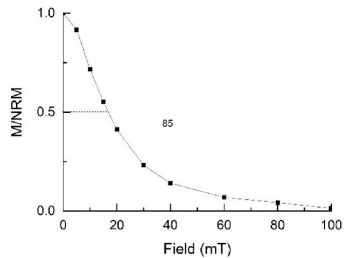


Figure 5

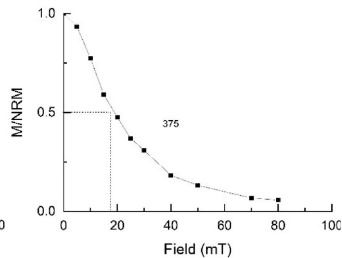
Sample 50-RV2



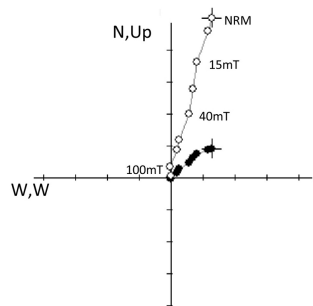
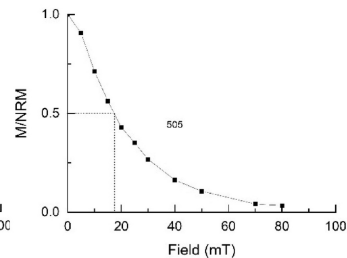
Sample 85-RV2



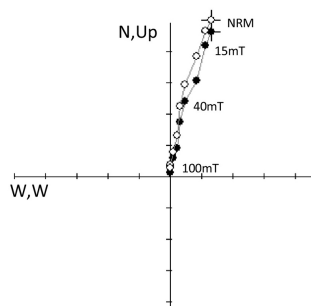
Sample 375-RV1



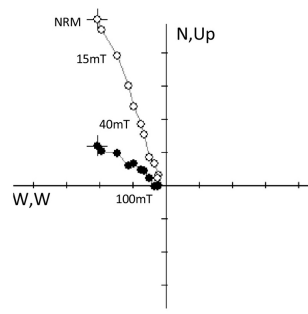
Sample 505-RV1



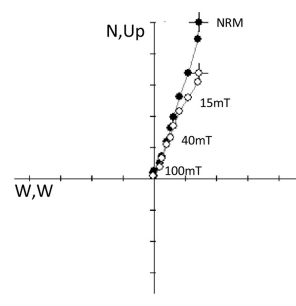
Declination: 53.1°
 Inclination: -71.9°
 MAD: 2.1°



Declination: 16.1°
 Inclination: -46.7°
 MAD: 3.2°



Declination: -59.1°
 Inclination: -64.4°
 MAD: 2.1°



Declination: 14.5°
 Inclination: -42.1°
 MAD: 3.2°

□ vertical projection

■ horizontal projection

Figure 6

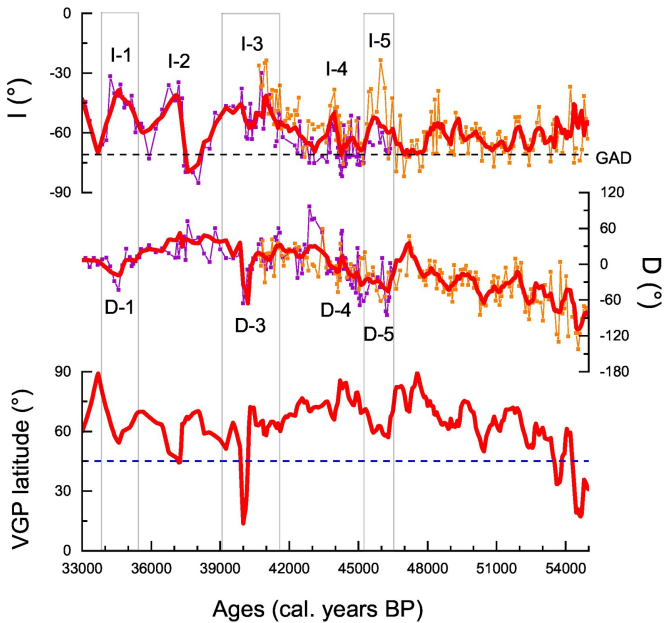


Figure 7

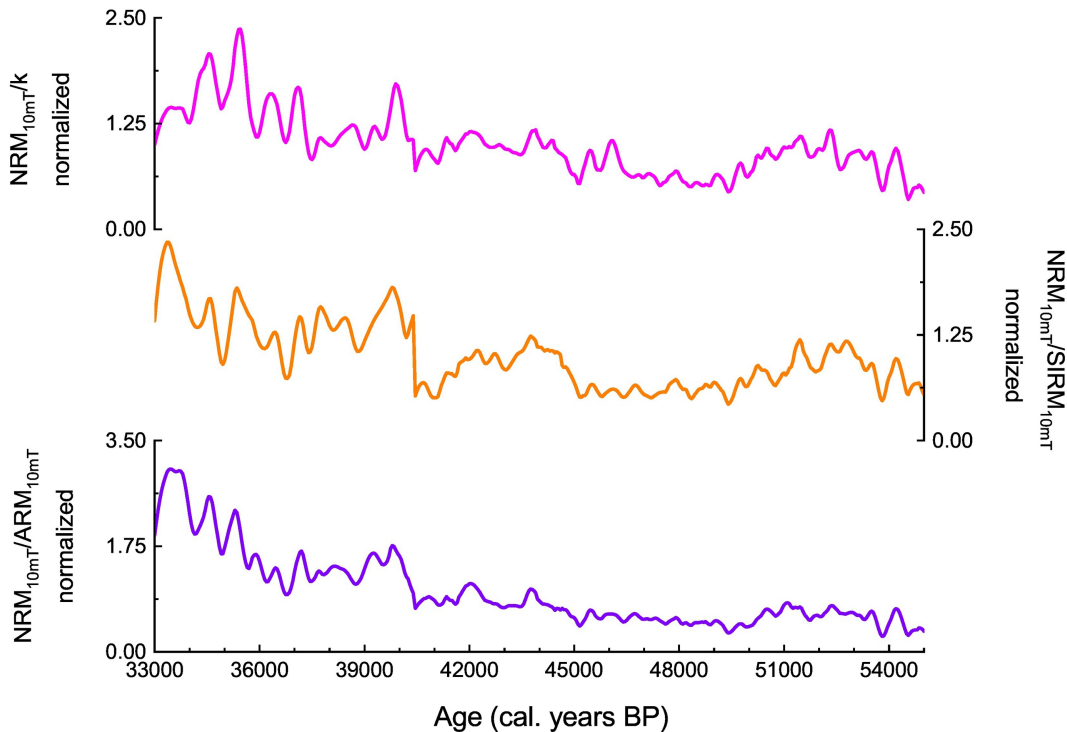


Figure 8

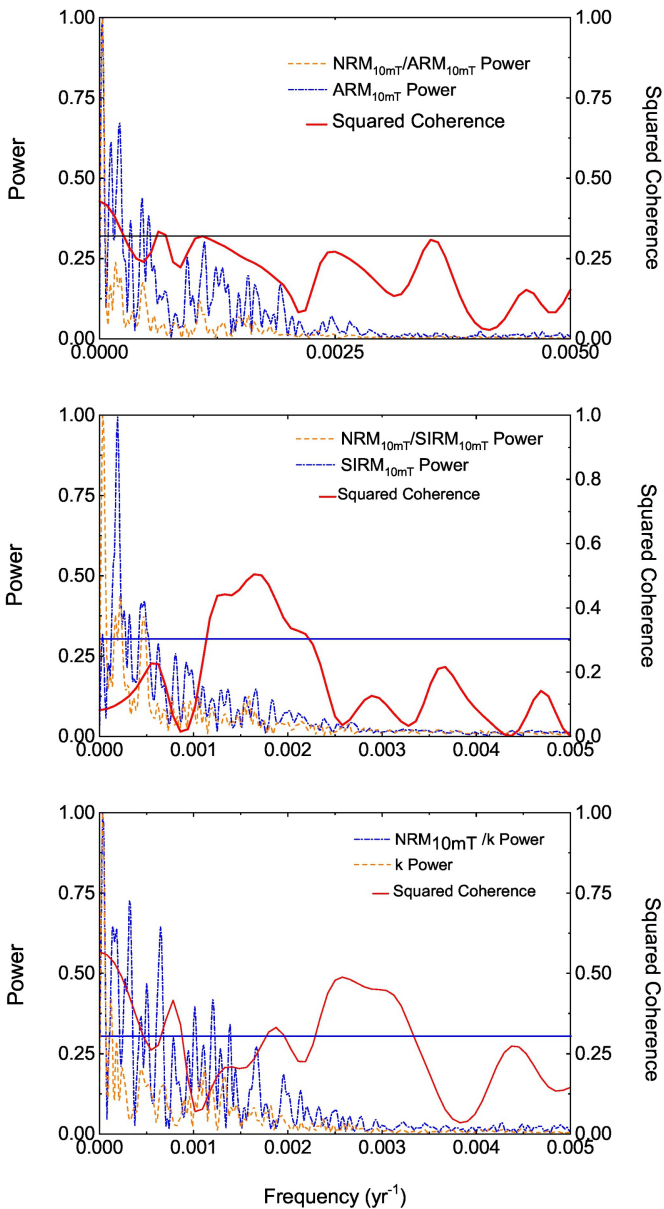
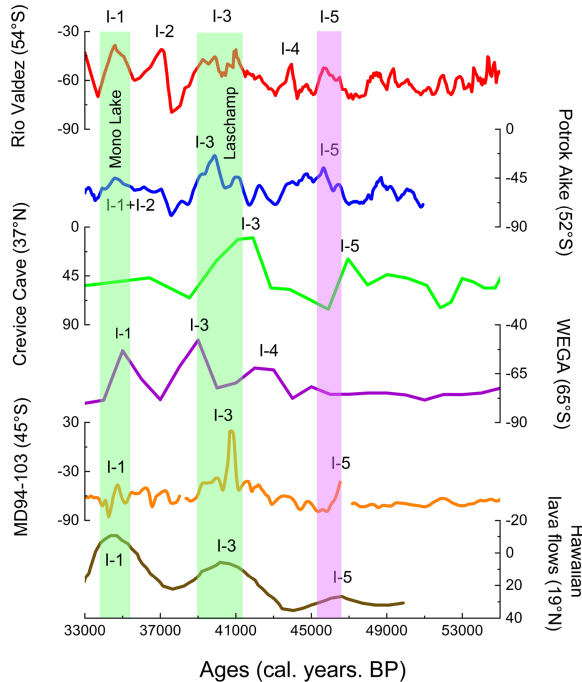
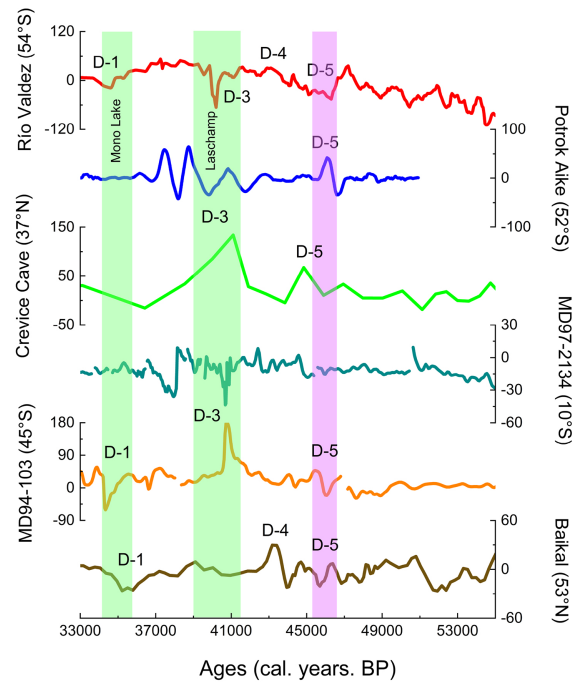


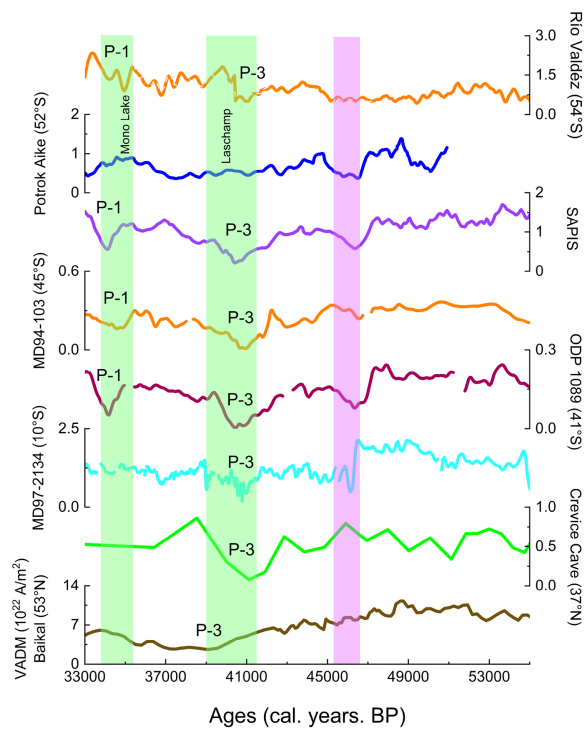
Figure 9



(a)



(b)



(c)

Figure 10